Journal of Materials Research and Technology 32 (2024) 4456–4464

Contents lists available at ScienceDirect

Journal of Materials Research and Technology

journal homepage: www.elsevier.com/locate/jmrt

Effect of V concentration in TiSiN monolayer coating on chip formation mechanism and chip sliding velocity during dry turning of Ti–6Al–4V alloy

Ch Sateesh Kumar [a,b,*], Gorka Urbikain [a,b], Pablo Fernández De Lucio [a,b], Cristian Pérez-Salinas [a,b], Luis Norberto López De Lacalle [a,b], Filipe Fernandes [c,d,**]

[a] CFAA- Aeronautics Advanced Manufacturing Centre, University of the Basque Country (UPV/EHU), Biscay Science and Technology Park, Ed. 202, Zamudio, Spain
[b] Department of Mechanical Engineering, University of the Basque Country, Escuela Superior de Ingenieros Alameda de Urquijo S/N, 48013, Bilbao, Spain
[c] University of Coimbra, CEMMPRE, ARISE, Department of Mechanical Engineering, Rua Luís Reis Santos, 3030-788 Coimbra, Portugal
[d] ISEP, Polytechnic of Porto, Rua Dr. António Bernardino de Almeida, 4249-015 Porto, Portugal

ARTICLE INFO

Keywords:
Chip sliding velocity
Chip flow angle
Chip formation mechanism
Self-lubricating coatings
TiSiVN coating

ABSTRACT

The current study examines how the self-lubricating characteristics of the novel TiSiVN coating affect the chip formation process and chip sliding velocity during the dry turning of Ti6Al4V titanium alloy. The serration bands tend to straighten at a cutting speed of 125 m/min, which is the main cause of the chips being straightened without tangling for both coated tools. TiSiVN coated tool accounts for higher chip sliding velocity due to the generation of lubricious phases, whereas the higher V_S for uncoated tool indicates high tool wear at the highest cutting speed of 125 m/min. Further, r and θ_n tend to have an inverse relationship with V_S, with 125 m/min cutting speed remaining an exception due to severe changes in tool wear dynamics. The reduction of friction helped to lower the localized strain along the shear bands and the effective stress at the beginning of the formation of the serrated tooth.

Abbreviations

h_{avg}	Average height of saw tooth
α	Orthogonal rake angle
β_s	Chip flow angle
V_S	Chip sliding velocity
V_C	Cutting velocity
i_s	Inclination angle
θ_n	Normal shear angle
r	Chip thickness ratio
α_n	Normal rake angle
p_{avg}	Average distance between two consecutive serrated teeth
τ_{cf}	Frictional stress
μ_{ap}	Apparent coefficient of friction
σ_N	Normal stress
σ_{Pmax}	Maximum principal stress
ε_f	Strain at fracture
ε	Equivalent strain
FSH_B	Free surface height of chip at the bottom
FSH_C	Free surface height of chip at the centre
FSH_T	Free surface height of chip at the top
FMH	Feed marks height
Z_N	Normal direction
Z_R	Rake direction
Z_C	Chip flow direction

1. Introduction

Titanium alloys are considered difficult to cut due to their low thermal conductivity and high chemical reactivity at high temperatures [1,2], resulting in high tool wear rates and poor surface quality of the machined surface [3]. Several attempts have been made to improve the machinability of titanium alloys, especially for Ti6Al4V alloy, one of the most widely used titanium alloys [4,5]. Thin-film depositions on the cutting tools are a widely used technique to improve the performance of cutting tools during machining [6–10]. Recently, self-lubricant coatings have been employed for machining applications. The benefit of these coating systems is the generation of lubricious phases like V_2O_5, WO_3, etc., which could help reduce friction and improve cutting tool

* Corresponding author. CFAA- Aeronautics Advanced Manufacturing Centre, University of the Basque Country (UPV/EHU), Biscay Science and Technology Park, Ed. 202, Zamudio, Spain.
** Corresponding author. University of Coimbra, CEMMPRE, ARISE, Department of Mechanical Engineering, Rua Luís Reis Santos, 3030-788 Coimbra, Portugal.
E-mail address: chigullasateesh.kumar@ehu.eus (C.S. Kumar).

https://doi.org/10.1016/j.jmrt.2024.09.007
Received 24 April 2024; Received in revised form 29 August 2024; Accepted 2 September 2024
Available online 3 September 2024

durability [11]. The solid lubricating properties of the Magnéli oxide phases of Ti, W, V, or Mo are attributed to their crystallographic planes with lower binding energy, which decreases friction [12]. The fast oxidation of coatings (such as AlCrSiVN and TiSiVN) and the subsequent generation of V_nO_{3n-1} (a low melting point lubricious phase) is primarily triggered by V inclusion to transition metal nitrides at elevated temperatures [13]. These self-lubrication properties are beneficial, especially when machining difficult-to-cut materials like Ti6Al4V alloy. Particularly, adding V to transition metal nitrides such as TiSiN and AlCrSiN leads to the release of low melting point lubricious phases at higher temperatures [13,14]. In this regard, TiSiVN coating enhanced the machining performance of the Al_2O_3/SiC tool due to the generation of V_2O_5 lubricious phase [15].

Furthermore, reports of a significant impact of thin-film depositions on cutting tools on chip formation and flow mechanics have been made. Additionally, the process of chip formation has a major impact on the tool wear on the rake surface [16,17]. Reportedly, Wang et al. [18] revealed that the cryogenic cooling techniques accounted for a reduction in chip thickness and an increase in tool wear. Similar machinability improvements and impact on chip formation mechanism due to cryogenic cooling were reported by Qiu et al. [19]. Additionally, chip sliding velocity affects the adhesion and friction behavior during machining [20]. It is reported that the thickness of AlCrN monolayer and AlTiN multi-layer coatings impact chip flow angles [16,21]. Further, it has been reported that chip geometrical parameters like chip serration frequency, chip thickness, and chip width are also affected by the coating depositions on cutting tools [17,22,23]. Also, it is inevitable to note that the chip formation impacts cutting friction, leading to the formation of a shear zone and, thus, affecting the machining forces [24].

From the literature survey, it is evident that the thin films and cooling techniques significantly impact the chip formation and chip flow mechanism. On the other hand, the impact of coatings' self-lubricating qualities on chip formation and chip flow mechanism has received little attention. Therefore, during the dry turning of Ti6Al4V titanium alloy, the current study will investigate how the self-lubricating properties of the TiSiVN coating affect chip formation and chip flow mechanisms.

2. Experimental methodology

The oblique cutting tests were performed on a CNC turning centre with Ti–6Al–4V having 35 ± 2 HRC hardness as the workpiece material (250 mm length, 100 mm diameter, and 100 mm cut length). The experiments were performed under a dry cutting environment with four different cutting speeds (50 m/min, 75 m/min, 100 m/min, and 125 m/min), constant feed rate (0.1 mm/rev), and depth of cut (0.5 mm). A 100 mm cut was made for each turning test. TiSiVN coated, TiSiN coated, and uncoated SiC-whiskers reinforced alumina (Al_2O_3) based cutting tools are used for cutting tests. Our previous work has elaborated on the coating deposition process [15]. The tool holder that was utilized in the experiments had an inclination angle (i_s) of 0° and orthogonal rake angle (α) of −8°. The chip geometry was determined using an Alicona non-contact 3D profilometer after the chips were mounted and polished. Later, to understand the chip formation mechanism more precisely, the machined and free surface of the chips were studied using a scanning electron microscope (SEM) equipped with electron dispersive spectroscopy (EDS). Further, topography analysis was also performed on the chips' free and machined surface using a 3D non-contact profilometer.

The schematic illustration of the oblique cutting process is shown in Fig. 1 where Z_N represents normal direction, Z_R represents rake direction, Z_C represents chip flow direction, α_n represents normal rake angle, and β_s represents chip flow angle. As shown in Fig. 2, the chip flow direction has been established by locating the sliding marks of the chips on the cutting tools. Further, the average saw tooth height (h_{avg}) and the average distance between two consecutive serrated teeth (p_{avg}) has been

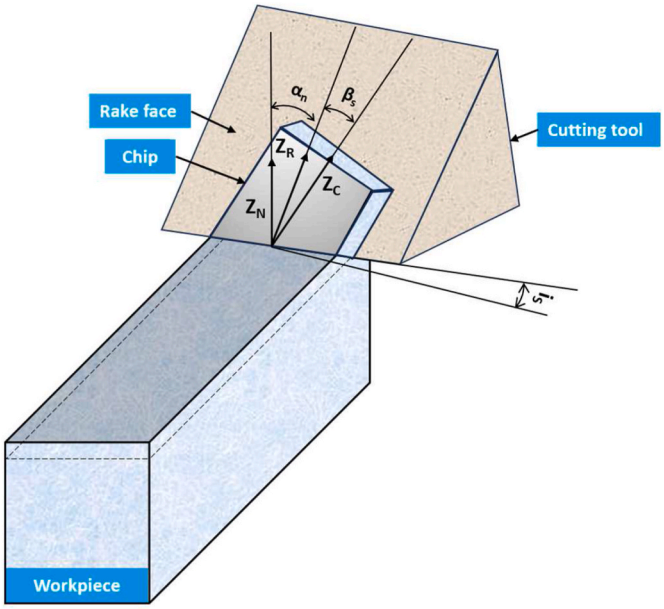

Fig. 1. A schematic representation of oblique cutting process.

measured on the thickness side of the chip, as shown in Fig. 3. A total of 20 measurements were made, and an average has been determined for both parameters. The calculation for both these geometrical parameters has been shown in equations (1) and (2).

$$h_{avg} = \frac{h_1 + h_2 + h_3 + h_4 + \ldots\ldots h_{20}}{20} \tag{1}$$

$$p_{avg} = \frac{p_1 + p_2 + p_3 + p_4 + \ldots\ldots\ldots p_{20}}{20} \tag{2}$$

After determining h_{avg} and p_{avg} the chip thickness ratio (r) was obtained using the below equation.

$$r = \frac{p_{avg}}{h_{avg}} \tag{3}$$

One of the most critical parameters to investigate is the chip sliding velocity which could help to understand adhesion, chip bending, and abrasive wear on the cutting tools [20]. The dependency of chip sliding velocity (V_S) on cutting velocity (V_C), normal shear angle (θ_n), inclination angle (i_s), chip flow angle (β_s), and normal rake angle (θ_n) is mathematically represented as [25]:

$$V_S = V_C \frac{\cos i_s \sin \theta_n}{\cos \beta_s \cos (\theta_n - \alpha_n)} \tag{4}$$

Where θ_n and α_n can be determined by the below equations [26].

$$\theta_n = tan^{-1}\left(\frac{r\left(\frac{\cos \beta_s}{\cos i_s}\right)\cos \alpha_n}{1 - r\left(\frac{\cos \beta_s}{\cos i_s}\right)\sin \alpha_n}\right) \tag{5}$$

$$\alpha_n = tan^{-1}(\cos i_s \tan \alpha) \tag{6}$$

Additionally, the localized stress and strain development in the serrated chips has been understood by the use of a 2D finite element created in Deform 2D (version 10.2). Deform 2D supports Lagrangian formulation that employs implicit integration for large deformations. Fig. 4 shows the schematic representation of the adopted 2D finite element model with boundary conditions. The edge radiuses were approximately 32 μm for uncoated and 41 μm for coated tools, respectively, consistent with the experimental cutting tools. The material

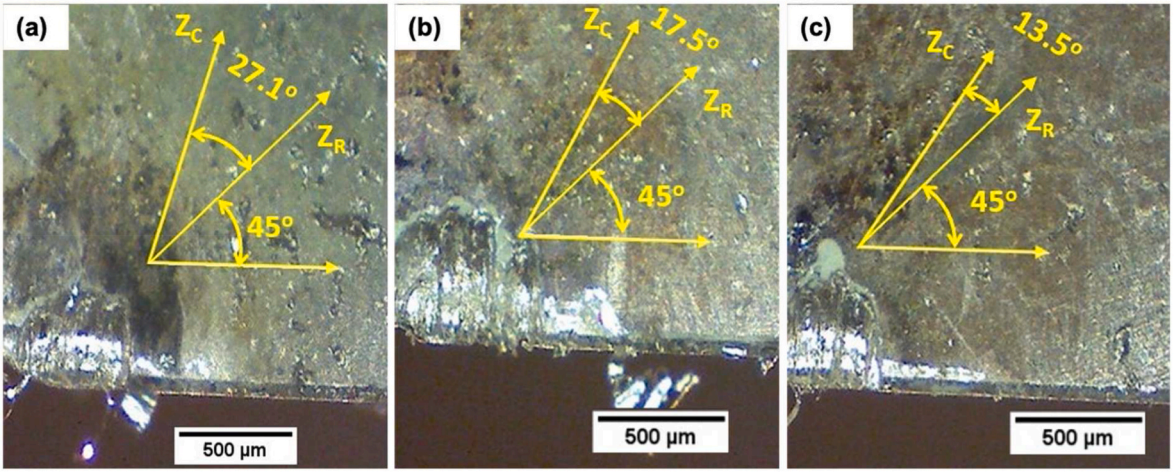

Fig. 2. Measurement of chip flow angle using chip sliding marks on (a) uncoated, (b) TiSiN coated and (c) TiSiVN coated cutting tool after machining at 50 m/min cutting speed.

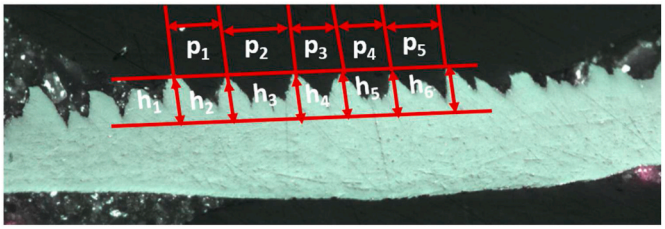

Fig. 3. Indicative measurement of saw tooth height and distance between two consecutive serrated teeth.

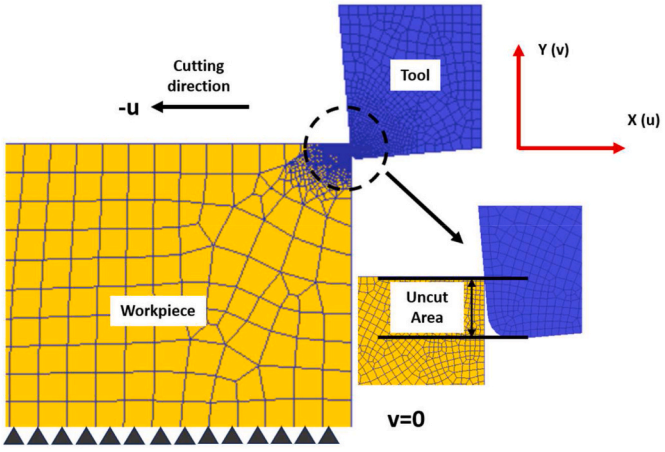

Fig. 4. 2D finite element model with boundary conditions.

properties of the tool and the workpiece have been taken from the Deform material database. The simulations were run based on the changes in the apparent coefficient of friction that were observed earlier [27] using a Coulomb's friction model [28] as shown in Equation (7). Mesh windows ensured a finer mesh at the chip formation zone and smooth re-meshing in the highly distorted zones. Thermally coupled quadrilateral elements were used to mesh both the tool and the workpiece. The cutting tool was meshed with approximately 700 elements whereas the workpiece is meshed with 2500 elements.

$$\tau_{cf} = \mu_{ap}\sigma_N \tag{7}$$

Where τ_{cf} is the frictional stress, μ_{ap} is the apparent coefficient of friction, and σ_N is the normal stress. The damage initiation in the chips is governed by Cockroft and Latham damage criterion (given by Equation (8)) [29] with critical damage value for fracture as 240 [30].

$$\int_0^{\varepsilon_f} \sigma_{Pmax} d\varepsilon = D \tag{8}$$

Where σ_{Pmax} is the maximum principal stress, ε_f is the strain at fracture, ε is the equivalent strain, and D is the critical damage value. According to Cockroft and Latham damage criterion, the chip segmentation begins when the integral of the maximum principal stress with respect to the equivalent plastic strain reaches the critical damage value. The model was validated using experimental cutting forces and chip geometry. An error of 5–10% was seen in the experimental and numerical results, which is acceptable.

3. Results and discussion

In this section, results related to the chip formation mechanism, chip geometrical parameters, free and back surface topography of the chips, and chip sliding velocity have been presented and discussed.

3.1. Chip formation mechanism

The optical microscope pictures of the chips produced when machining with TiSiVN and TiSiN coated, and uncoated cutting tools are displayed in Fig. 5. At 50 m/min, the chips formed corresponding to all cutting tools were continuous in the form of long curls with well-defined curl diameters. However, the increase of cutting speed to 75 m/min and above results in chips that are snarled. The chips for uncoated tools tend to bend and form tightened strings, which is also the case for coated tools till 100 m/min. This entanglement is caused by the increase in cutting temperature and material adhesion on the tool face as the cutting speed increases, which results in the sticking of chips on the tool face, causing an increase in chip bending angle. Interestingly at a cutting speed of 125 m/min, the chips for coated tools are more straightened without bends, whereas, for uncoated tools, tangling is reduced. This phenomenon can be attributed to the reduced chip bend angles at this cutting speed of 125 m/min, which prevented the tangling of the chips during their movement over the tool face [15].

Figs. 6 and 7 illustrate the SEM micrographs of the chips' free and back surfaces to help better comprehend this phenomenon. The free surface of the chips constitutes both primary and secondary serrated teeth. Further, the increase in cutting speed causes the secondary serration to be more prominent due to the increased cutting

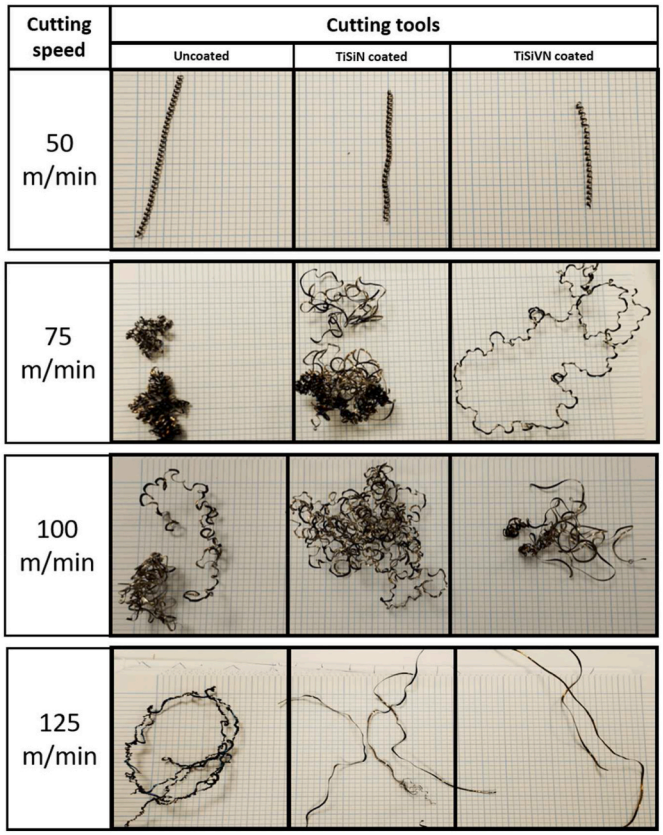

Fig. 5. Optical microscopy images showing chip formation during machining with uncoated, and TiSiN and TiSiVN coated cutting tools.

temperature, which causes easy movement of the serrated planes. The primary serration bands tend to bulge outside with increased cutting speed mainly because of increased temperature. However, the serration bands tend to straighten at a cutting speed of 125 m/min, which is a primary reason for straightened chips without tangling for TiSiVN and TiSiN coated tools. The previously observed chip bend angles, which both rely on the cutting temperature and the crater depth increment with increasing cutting speed, can be directly connected to this straightening of the chips.

The back side, or machined surface, of the chips created during machining with coated and uncoated tools is seen in Fig. 7. The back surface shows the formation of feed marks due to smearing. But with the TiSiVN coated tools, the smearing decreased at higher cutting speed primarily because of the better machining performance ascribed to the development of V_2O_5 lubricious phases, which lower friction at high cutting temperatures [15,31]. Conversely, with the uncoated cutting tools, smearing gets worse as cutting speed rises. Further, there are clear signs of diffusion (see Fig. 8), with the EDS analysis showing the presence of tool material (Al) on the chips. However, the height of feed marks would be an interesting phenomenon to be studied, which will be discussed in section 3.2.

3.2. Back (machined) and free surface topography

Fig. 9 illustrates the axes on which the topography measurements have been made. XX and X'X' represent two axes out of the 20 axes that were considered for measuring the height of feed marks (FMH). On the contrary, YY, Y'Y', and Y''Y'' represent axes for the measurement of free surface height at the centre (FSH_C), top (FSH_T), and bottom (FSH_B), respectively. In Fig. 10, all of the data for FSH_B, FSH_C, FSH_T, and FMH have been plotted versus cutting speed. FSH_C decreases and then remains in the same level. The initial drop is due to the rise in temperature with cutting speed causing lower deformation of chips. However, a slight increase in FSH_C is seen for TiSiVN coated tools at higher cutting speeds. This may be due to the combined effect of preservation of effective cutting edge and reduction of the lubricious effect of the V_2O_5 phase at higher cutting speeds [27].

However, no further decrease is seen as the excessive adhesion at higher cutting temperatures would cause more slipping of the chip segments. On the contrary, FSH_B and FSH_T exhibit an inverse trend indicating shifting of serration from bottom to top with increased cutting speed. This trend is closely related to increased chip bend angles and crater height with the cutting speed [15]. The developed chips tend to move in a direction away from the tool face. However, with the increase in adhesion, the chip's bottom part remains in contact with the tool face for a more extended period, resulting in more sliding of the chip segments on the top. Additionally, as a result of the deeper crater depth, the chip bends and presses against the tool face on the bottom side, making it easier for chip segments to slide across the top. FMH exhibits a similar tendency of decreasing with increasing cutting speed. Because a chip's contact time with the tool face is reduced at a specific spot, a higher cutting speed reduces smearing on the machined surface. Thus, the

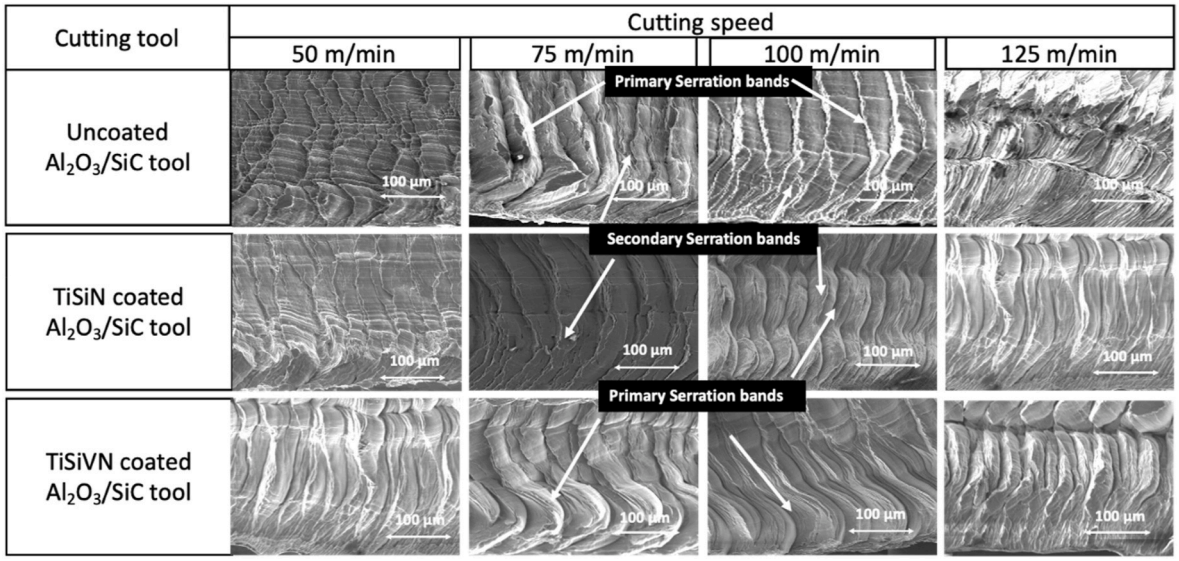

Fig. 6. SEM micrographs of the free surface of the chips.

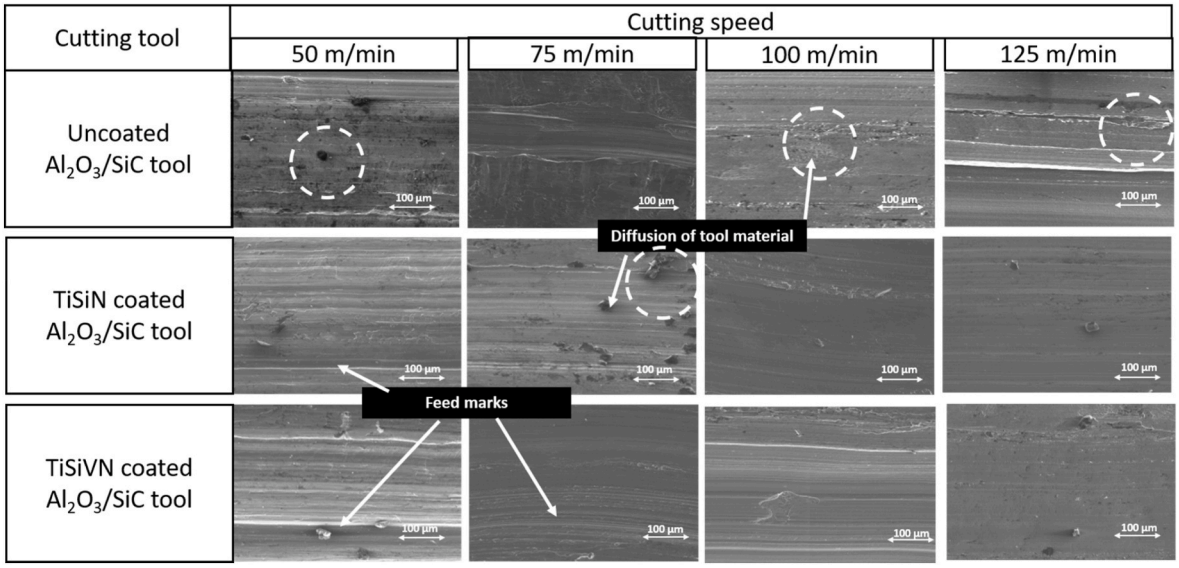

Fig. 7. SEM micrographs of the back (machined) surface of the chips.

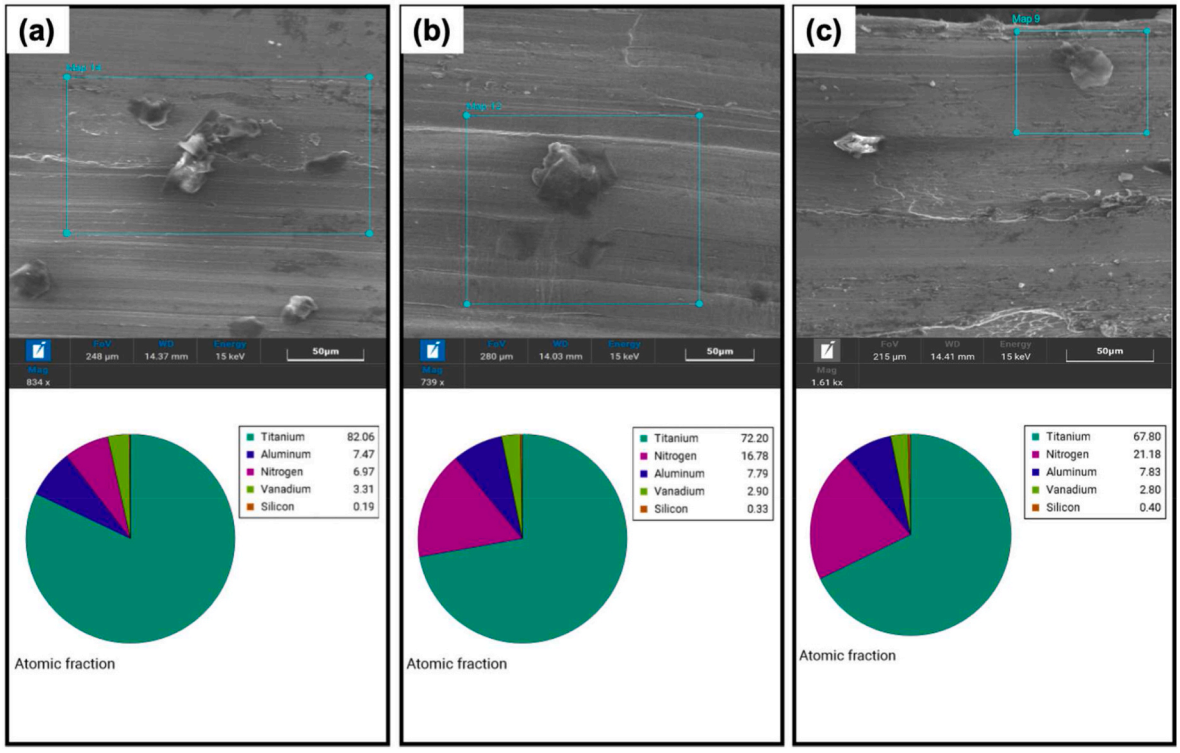

Fig. 8. EDS atomic fraction analysis of the machined surface of the chips corresponding to (a) uncoated, (b) TiSiN coated, and (c) TiSiVN coated tools.

stacking of chip material due to sliding friction reduces, leading to decreased FMH. Further, the TiSiVN coated tool exhibits lower values of FMH due to the generation of lubricious phases causing reduction of friction, which is also a reason for lower FSH_B, FSH_C, and FSH_T for TiSiVN coated tool in comparison to TiSiN coated and uncoated cutting tool.

3.3. Chip geometrical parameters

Fig. 11 shows the variation of the h_{avg}, p_{avg}, and β_s with cutting speed. The h_{avg} remains mainly on the same level till 75 m/min, after which the trend changes. For the uncoated tool, h_{avg} decreases whereas for the coated tool, it increases with further cutting speed. This trend can be related to the drastic decrease of effective cutting edge at 125 m/min for uncoated tool, with a significant rise in adhesion at the chip-tool interface for coated tools [15]. TiSiVN coated and TiSiN coated tools correspond to higher values of h_{avg} and p_{avg} compared to uncoated tools due to superior wear resistance properties. Conversely, p_{avg} decreased as cutting speed increased, which is consistent with other research that indicates a rise in serration frequency as cutting speed increases, resulting in a shorter gap between two successive serrated teeth [32,33]. Additionally, as cutting speed reaches 100 m/min, the chip flow angle (β_s) rises. This might be attributed to a rise in temperature and consequent material adhesion at the chip-tool interface. Nevertheless, at 125

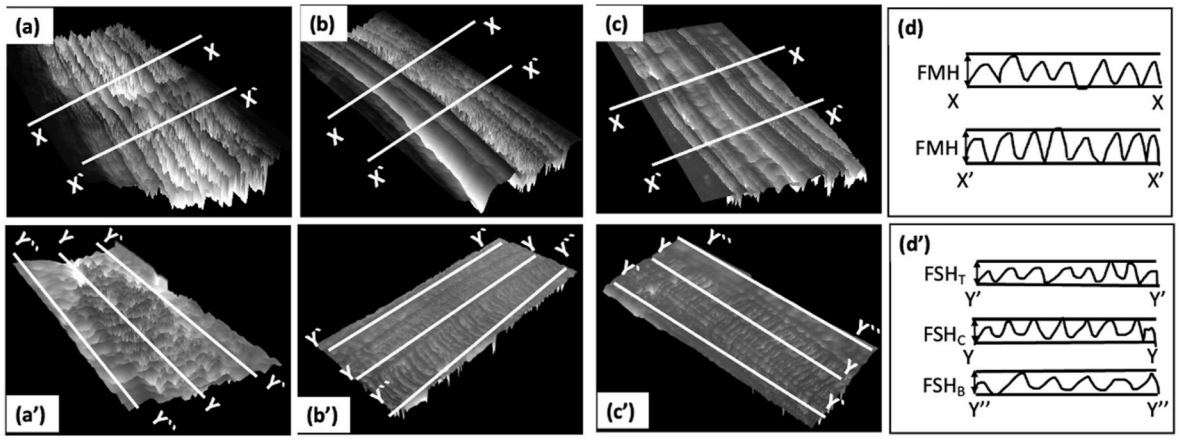

Fig. 9. Profilometer topography representing measurements on machined (back) surface [(a) uncoated, (b) TiSiN coated, and (c) TiSiVN coated] and free surface [(a') uncoated, (b') TiSiN coated, and (c') TiSiVN coated] of chips formed during machining at 50 m/min cutting speed, (d) indicative measurement of FHM along X-X and X′-X′ axes and (d') indicative measurement of FSH_T, FSH_C, and FSH_B along Y′-Y′, Y–Y and Y″-Y″ axes respectively.

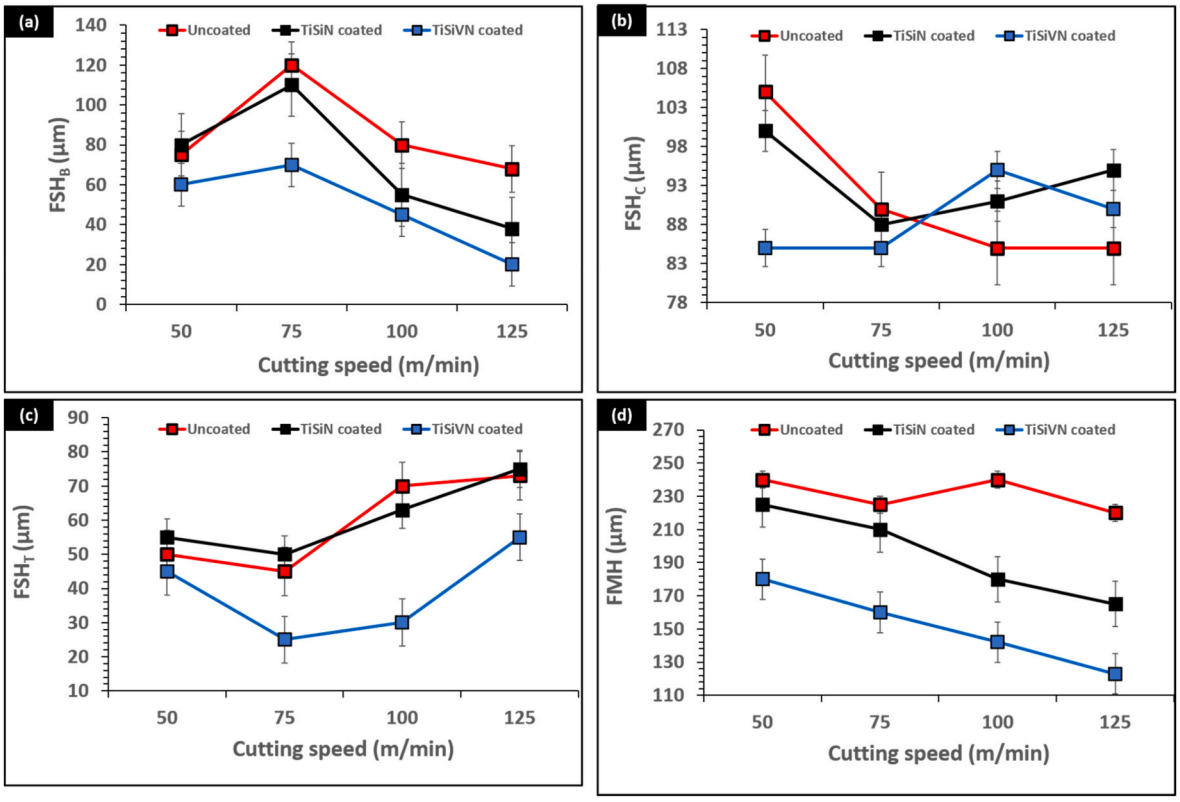

Fig. 10. Variation of (a) FSH_B, (b) FSH_C, (c) FSH_T, and (d) FMH with cutting speed.

m/min, the β_s decreases because of the rise in crater depth reported earlier [15]. Lower adhesion at the chip-tool contact is specified by the lower chip flow angles for the TiSiVN coated tool. Further, reduced adhesion for TiSiVN coated tools is caused by the lubrication produced by the generation of V_2O_5 self-lubricating phases at the chip-tool interface.

3.4. Normal shear angle and chip sliding velocity

The calculated values of V_S, θ_n, and r are presented in Table 1 and have also been plotted versus cutting speed in Fig. 12. It's interesting to note that r and θ_n decreases till the cutting speed of 100 m/min for uncoated tool and rise at 125 m/min cutting speed. Conversely, they reduce when cutting speed rises for coated tools. The lowering of the shear angle is linked to the thermal softening of the workpiece material as the cutting speed increases.

Further, lowering of shear angle can cause an increase in machining forces and tool wear [34]. However, the increase in shear angle for uncoated tools indicates catastrophic failure or significant reduction of effective cutting edge, causing a reduction of machining forces [15]. On the contrary, the V_S increases with cutting speed; thus, cutting speed is the dominant factor affecting V_S. However, interestingly, a decrease in V_S can be seen at 125 m/min for both coated tools. This decrease can be related to increased adhesion levels at higher cutting speeds for coated tools.

Further, the high cutting temperatures prevailing at 125 m/min

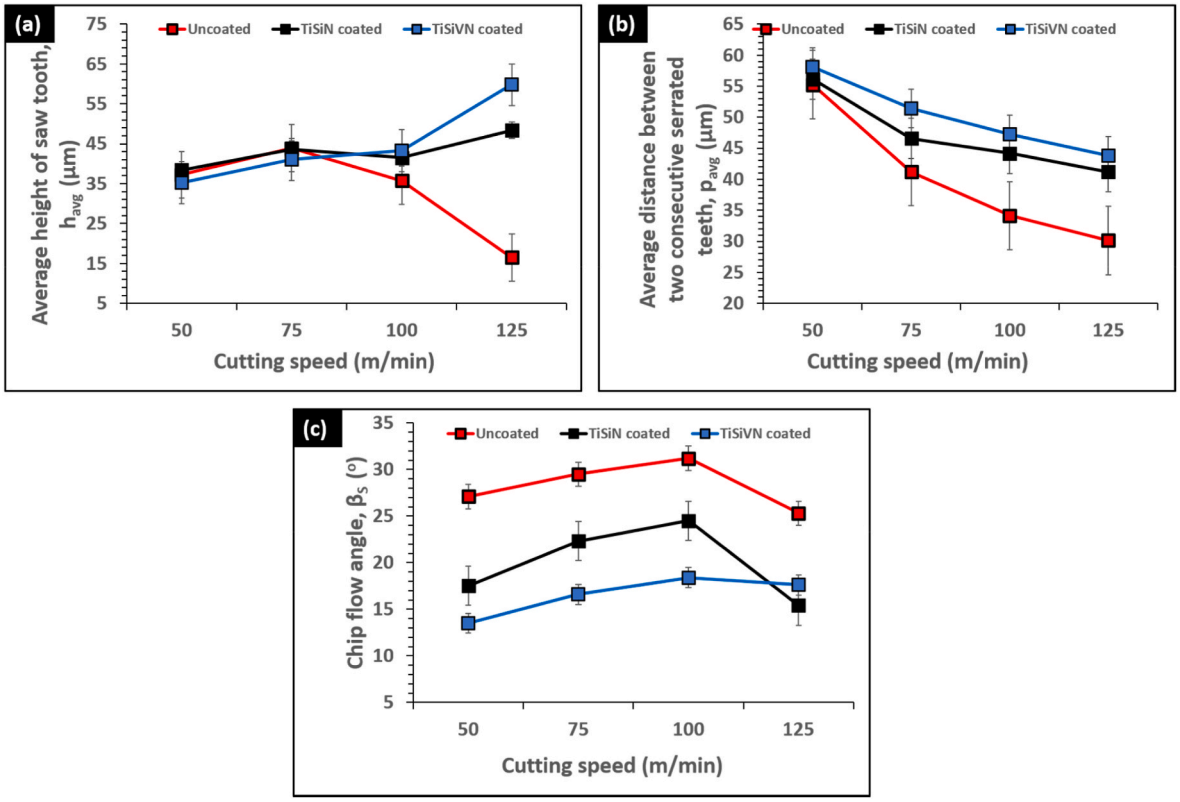

Fig. 11. Variation of (a) h_{avg}, (b) p_{avg}, and (c) chip flow angle β_s with cutting speed.

Table 1
Evaluated values of average saw tooth height, average distance between two consecutive serrated teeth, chip flow angle, chip thickness ratio, normal shear angle and chip sliding velocity.

Cutting tool	V_C (m/min)	h_{avg} (µm)	p_{avg} (µm)	β_s (°)	r	θ_n (°)	V_S (m/min)
Al_2O_3/SiC uncoated	50	37.23	55.22	27.1	1.48	47.84	74.16
TiSiN coated		38.45	56.12	17.5	1.46	49.11	72.98
TiSiVN coated		35.18	58.06	13.5	1.65	52.41	82.52
Al_2O_3/SiC uncoated	75	43.88	41.21	29.5	0.94	36.01	70.44
TiSiN coated		43.61	46.55	22.3	1.07	40.69	80.06
TiSiVN coated		41.12	51.43	16.6	1.25	45.49	93.80
Al_2O_3/SiC uncoated	100	35.75	34.12	31.2	0.95	35.98	95.44
TiSiN coated		41.5	44.16	24.5	1.06	40.20	106.41
TiSiVN coated		43.22	47.21	18.4	1.09	41.89	109.23
Al_2O_3/SiC uncoated	125	16.5	30.14	25.3	1.83	53.06	132.21
TiSiN coated		48.38	41.19	15.4	0.85	36.11	83.26
TiSiVN coated		59.76	43.77	17.6	0.73	32.22	77.52

cutting speed would cause complete coating oxidation in the cutting zone, seizing almost all beneficial effects of coatings. Notably, the TiSiVN coated tool accounts for higher V_S due to the generation of lubricious phases causing faster sliding of the chips on the tool surface. On the contrary, an increase of V_S for the uncoated tool indicates high tool wear, causing wear of effective cutting edge at 125 m/min cutting speed, which has been reported earlier [27]. Further, r and θ_n tend to have an inverse relationship with V_S, with 125 m/min cutting speed remaining an exception due to severe changes in tool wear dynamics [27].

3.5. Stress and strain along shear bands

Fig. 13 illustrates the development of stress and strain along a localized region of the shear band in the serrated teeth during machining. The reduction of friction tends to reduce effective strain along the adiabatic shear band. The higher strain would lead to an increase in saw tooth height. Further, a higher strain along the shear band would account for the premature bending of the chips, preventing the formation of well-defined curls, which was reported in section 3.1. However, the measured saw tooth height (see Table 1) shows that tool wear is the dominant parameter affecting chip thickness [27]. Also, the effective stress at the beginning of the formation of the serrated tooth is higher towards the tip for a higher value of the coefficient of friction, which has been shown in the marked region. The greater chip flow angles and shorter spacing between the serrated teeth may occur from the chip being pushed forward by the elevated stress levels at the tip of the serrated teeth. Thus, the uncoated tool always corresponds to higher values of p_{avg} and β_s.

4. Conclusions

The current study examines how the self-lubricating properties of the TiSiVN coating affect the chip formation mechanism and sliding velocity. The results that have been presented leads to the following conclusions.

1. The primary serration bands tend to bulge outside with increased cutting speed mainly because of increased temperature. However, the serration bands tend to straighten at the cutting speed of 125 m/

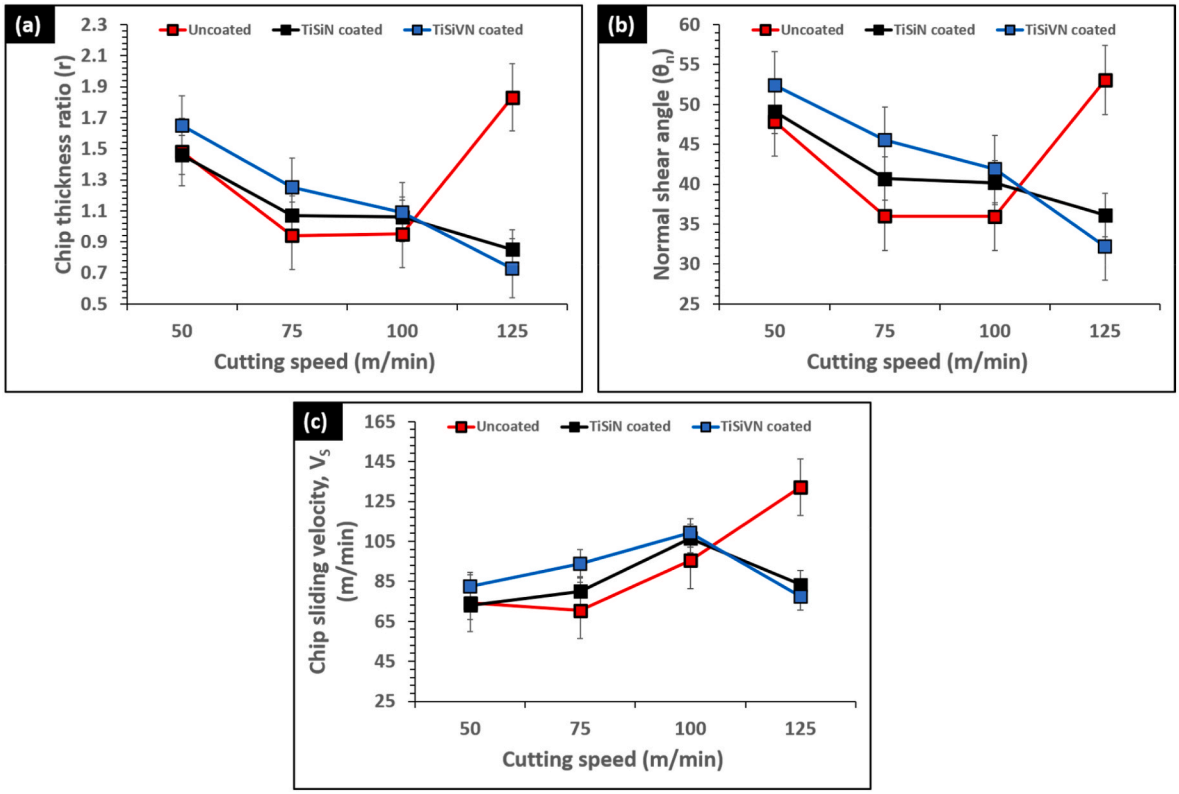

Fig. 12. Variation of (a) chip thickness ratio (r), (b) normal shear angle (θ_n), and (c) chip sliding velocity (V_S) with cutting speed.

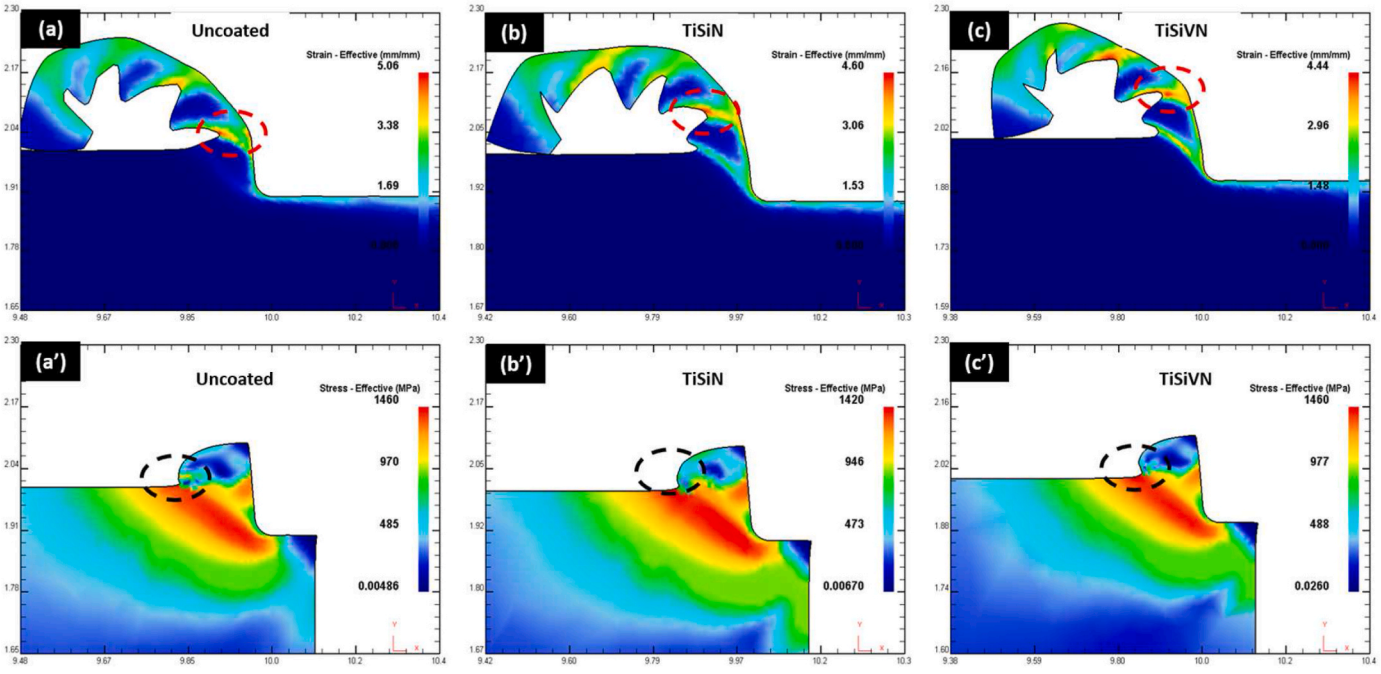

Fig. 13. Localized strain (a, b, and c) and localized stress (a', b', and c') in uncoated and coated cutting tools.

min, which is a primary reason for straightened chips without tangling for the coated tools. This straightening of chips can be directly linked to the chip bend angles reported earlier, which further depend on the cutting temperature and crater depth increment with increased cutting speed.

2. When compared to TiSiN coated and uncoated cutting tools, the TiSiVN coated tool displays lower values of FMH because the production of lubricious phases that accounts to the reduction of friction. This is also the cause of lower FSH_B, FSH_C, and FSH_T for the TiSiVN coated tool.
3. The rise in temperature and the accompanying increase in the adhesion of workpiece material at the chip-tool interface with cutting speed may be the primary reason for the chip flow angle's (β_s)

increase with cutting speed up to 100 m/min. However, β_s decreases at 125 m/min because the crater depth increases.

4. The reduction of friction helped in lowering the localized strain along the shear bands. Also, the effective stress at the beginning of the formation of the serrated tooth is higher towards the tip for a higher value of the coefficient of friction.
5. The TiSiVN coated tool accounts for higher V_S due to the generation of lubricous phases whereas the higher V_S for the uncoated tool indicates high tool wear at the cutting speed of 125 m/min. Further, r and θ_n tend to have an inverse relationship with $V_{S,}$ with 125 m/min cutting speed remaining an exception due to severe changes in tool wear dynamics.

Declaration of competing interest

The authors declare that they have no known competing financial interests or personal relationships that could have appeared to influence the work reported in this paper.

Acknowledgements

Thanks are also to Basque Government for funding Excellence University groups IT 1573-22. Experimental testing was based in results projectPID2022-137380OB-I00 NEOPHYM, by Spanish MINECO and Spanish research Agency (MCIN/AEI/10.13039/501100011033.Thanks are also send to regional project and Basque government in projects: ORLEGI and ECOVERSO. Filipe Fernandes acknowledges the UIDB/00285/2020 and LA/P/0112/2020 projects, sponsored by FEDER Funds through Portugal 2020 (PT2020), the Competitiveness and Internationalization Operational Program (COMPETE 2020), and national funds through the Portuguese Foundation for Science and Technology (FCT).

References

[1] Venugopal KA, Paul S, Chattopadhyay AB. Growth of tool wear in turning of Ti-6Al-4V alloy under cryogenic cooling. Wear 2007;262:1071–8. https://doi.org/10.1016/j.wear.2006.11.010.
[2] Hosseini A, Kishawy HA. Machining of titanium alloys. https://doi.org/10.1007/978-3-662-43902-9; 2014.
[3] Jamil M, Zhao W, He N, Gupta MK, Sarikaya M, Khan AM, R SM, Siengchin S, Pimenov DY. Sustainable milling of Ti–6Al–4V: a trade-off between energy efficiency, carbon emissions and machining characteristics under MQL and cryogenic environment. J Clean Prod 2021;281:125374. https://doi.org/10.1016/j.jclepro.2020.125374.
[4] Shokrani A, Al-Samarrai I, Newman ST. Hybrid cryogenic MQL for improving tool life in machining of Ti-6Al-4V titanium alloy. J Manuf Process 2019;43:229–43. https://doi.org/10.1016/j.jmapro.2019.05.006.
[5] Ozel T, Sima M, Srivastava AK, Kaftanoglu B. Investigations on the effects of multi-layered coated inserts in machining Ti-6Al-4V alloy with experiments and finite element simulations. CIRP Ann Manuf Technol 2010;59:77–82. https://doi.org/10.1016/j.cirp.2010.03.055.
[6] Liu W, Chu Q, Zeng J, He R, Wu H, Wu Z, Wu S. PVD-CrAlN and TiAlN coated Si_3N_4 ceramic cutting tools -1. Microstructure, turning performance and wear mechanism. Ceram Int 2017;0–1. https://doi.org/10.1016/j.ceramint.2017.04.041.
[7] Keunecke M, Stein C, Bewilogua K, Koelker W, Kassel D, van den Berg H. Modified TiAlN coatings prepared by d.c. pulsed magnetron sputtering. Surf Coat Technol 2010;205:1273–8. https://doi.org/10.1016/j.surfcoat.2010.09.023.
[8] Yang W, Xiong J, Guo Z, Du H, Yang T, Tang J, Wen B. Structure and properties of PVD TiAlN and TiAlN/CrAlN coated Ti(C, N)-based cermets. Ceram Int 2016;43:1911–5. https://doi.org/10.1016/j.ceramint.2016.10.151.
[9] Rech J. Influence of cutting tool coatings on the tribological phenomena at the tool-chip interface in orthogonal dry turning. Surf Coat Technol 2006;200:5132–9. https://doi.org/10.1016/j.surfcoat.2005.05.032.
[10] Kumar CS, Patel SK. Investigations on the effect of thickness and structure of AlCr and AlTi based nitride coatings during hard machining process. J Manuf Process 2018;31:336–47. https://doi.org/10.1016/j.jmapro.2017.11.031.
[11] Mulligan CP, Gall D. CrN-Ag self-lubricating hard coatings. Surf Coat Technol 2005;200:1495–500. https://doi.org/10.1016/j.surfcoat.2005.08.063.
[12] Al-rjoub A, Bin T, Cavaleiro A, Fernandes F. The influence of V addition on the structure , mechanical properties , and oxidation behaviour of TiAlSiN coatings deposited by DC magnetron sputtering. J Mater Res Technol 2022;20:2444–53. https://doi.org/10.1016/j.jmrt.2022.08.009.
[13] Franz R, Mitterer C. Vanadium containing self-adaptive low-friction hard coatings for high-temperature applications: a review. Surf Coat Technol 2013;228:1–13. https://doi.org/10.1016/j.surfcoat.2013.04.034.
[14] Fernandes F, Oliveira JC, Cavaleiro A. Self-lubricating TiSi(V)N thin films deposited by deep oscillation magnetron sputtering (DOMS). Surf Coat Technol 2016;308:256–63. https://doi.org/10.1016/j.surfcoat.2016.07.039.
[15] Kumar CS, Urbikain G, de Lacalle LNL, Gangopadhyay S, Fernandes F. Investigating the effect of novel self-lubricant TiSiVN films on topography, diffusion and oxidation phenomenon at the chip-tool interface during dry machining of Ti-6Al-4V alloy. Tribol Int 2023;186. https://doi.org/10.1016/j.triboint.2023.108604.
[16] Sateesh Kumar C, Kumar Patel S. Hard machining performance of PVD AlCrN coated Al2O3/TiCN ceramic inserts as a function of thin film thickness. Ceram Int 2017;43:13314–29. https://doi.org/10.1016/j.ceramint.2017.07.030.
[17] An Q, Wang C, Xu J, Liu P, Chen M. Experimental investigation on hard milling of high strength steel using PVD-AlTiN coated cemented carbide tool. Int J Refract Metals Hard Mater 2014;43:94–101. https://doi.org/10.1016/j.ijrmhm.2013.11.007.
[18] Wang R, Wang X, Yan P, Zhou T, Jiao L, Teng L, Zhao B. The effects of cryogenic cooling on tool wear and chip morphology in turning of tantalum-tungsten alloys Ta-2.5W. J Manuf Process 2023;86:152–62. https://doi.org/10.1016/j.jmapro.2022.12.063.
[19] Qiu W, Pan D, Li J, Guo P, Qiao Y, Wang X. Chip formation mechanism in cryogenic machining of high temperature alloy-Inconel 718 and Ti-47.5Al-2.5V-1.0Cr. J Manuf Process 2023;97:35–47. https://doi.org/10.1016/j.jmapro.2023.04.060.
[20] Kumar CS, Patel SK. Effect of chip sliding velocity and temperature on the wear behaviour of PVD AlCrN and AlTiN coated mixed alumina cutting tools during turning of hardened steel. Surf Coat Technol 2017;334:509–25. https://doi.org/10.1016/j.surfcoat.2017.12.013.
[21] Kumar CS, Patel SK. Experimental and numerical investigations on the effect of varying AlTiN coating thickness on hard machining performance of Al 2 O 3 -TiCN mixed ceramic inserts. Surf Coat Technol 2017;309:266–81. https://doi.org/10.1016/j.surfcoat.2016.11.080.
[22] Thakur A, Gangopadhyay S, Mohanty A. Investigation on some machinability aspects of inconel 825 during dry turning. Mater Manuf Process 2015;30:1026–34. https://doi.org/10.1080/10426914.2014.984216.
[23] Jiang F, Yan L, Rong Y. Orthogonal cutting of hardened AISI D2 steel with TiAlN-coated inserts - simulations and experiments. Int J Adv Manuf Technol 2013;64:1555–63. https://doi.org/10.1007/s00170-012-4122-3.
[24] Liang X, Liu Z, Wang B, Wang C, Cheung CF. Friction behaviors in the metal cutting process: state of the art and future perspectives. Int J Extrem Manuf 2023;5. https://doi.org/10.1088/2631-7990/ac9e27.
[25] Moufki A, Dudzinski D, Molinari A, Rausch M. Thermoviscoplastic modelling of oblique cutting : forces and chip # ow predictions, vol. 42; 2000. p. 1205–32.
[26] Journal AI, Aksu B, Çelebi C, Budak E. An experimental investigation of oblique cutting mechanics. 0344, https://doi.org/10.1080/10910344.2016.1196458; 2017.
[27] Kumar CS, Urbikain G, De Lucio PF, De Lacalle LNL, Pérez-Salinas C, Gangopadhyay S, Fernandes F. Investigating the self-lubricating properties of novel TiSiVN coating during dry turning of Ti6Al4V alloy. Wear 2023:532–3. https://doi.org/10.1016/j.wear.2023.205095.
[28] Li K, Gao XL, Sutherland JW. Finite element simulation of the orthogonal metal cutting process for qualitative understanding of the effects of crater wear on the chip formation process. J Mater Process Technol 2002;127:309–24. https://doi.org/10.1016/S0924-0136(02)00281-9.
[29] Senthilkumar N, Tamizharasan T. Effect of tool geometry in turning AISI 1045 steel: experimental investigation and FEM analysis. Arab J Sci Eng 2014;39:4963–75. https://doi.org/10.1007/s13369-014-1054-2.
[30] Lu J, Chen J, Fang Q, Liu B, Liu Y, Jin T. Finite element simulation for Ti-6Al-4V alloy deformation near the exit of orthogonal cutting. Int J Adv Manuf Technol 2016;85:2377–88. https://doi.org/10.1007/s00170-015-8077-z.
[31] Fernandes F, Morgiel J, Polcar T, Cavaleiro A. Oxidation and diffusion processes during annealing of TiSi(V)N films. Surf Coat Technol 2015;275:120–6. https://doi.org/10.1016/j.surfcoat.2015.05.031.
[32] Wang B, Liu Z. Investigations on the chip formation mechanism and shear localization sensitivity of high-speed machining Ti6Al4V. Int J Adv Manuf Technol 2014;75:1065–76. https://doi.org/10.1007/s00170-014-6191-y.
[33] Wang B, Liu Z, Hou X, Zhao J. Influences of cutting speed and material mechanical properties on chip deformation and fracture during high-speed cutting of inconel 718. Materials 2018;11. https://doi.org/10.3390/ma11040461.
[34] Brown CA. Machining of metals: fundamentals. Encyclopedia of Materials: Sci Technol 2001:4703–8. https://doi.org/10.1016/b0-08-043152-6/00820-2.